Int. J. Electrochem. Sci., 13 **(2018)** 9905 – 9915, doi: 10.20964/2018.10.29

International Journal of ELECTROCHEMICAL SCIENCE
www.electrochemsci.org

Vanadium pentoxide and tungsten oxide as substrates for enzyme immobilization in an EGFET-biosensor

Elidia Maria Guerra[1*], *Dane Tadeu Cestarolli*[1] *and Marcelo Mulato*[2]

[1] Department of Chemistry, Biotechnology and Bioprocess Engineering, Federal University of São João Del Rei, Ouro Branco, MG, Brazil
[2] Department of Physics, FFCLRP-USP, Av. Bandeirantes, 3900, 14040-901, Ribeirão Preto, SP, Brazil
[*]E-mail: elidiaguerra@ufsj.edu.br

Received: 26 January 2018 / *Accepted:* 28 July 2018 / *Published:* 1 September 2018

V_2O_5 and WO_3 were obtained via sol-gel process as candidates to application in biosensors. X-ray diffractograms indicated the presence of lamellar structures, d = 1.17 nm and d = 0.69 nm, corresponding to $V_2O_5.1.8H_2O$ and $WO_3.2H_2O$, respectively. SEM images of V_2O_5 in xerogel form (comment 2) revealed a vanadium pentoxide xerogel ribbons with one dimensional stacking . Diffractogramms corresponding to WO_3 in xerogel form (comment 2) revealed a delamination process, which resulted in an irregular stack of rounded platelets. Investigation of the electronic and electrochemical properties of the samples was conducted using cyclic voltammetry (CV) and extended gate field effect transistors (EGFET). Glucose oxidase (GOx) was further immobilized to act as the sensing component in a biosensor. CV and EGFET were also used to confirm immobilization of GOx on the oxide surfaces, indicating that the materials are promising candidates for application as disposable biosensors in the future.

Keywords: V_2O_5; WO_3; glucose oxidase; Cyclic Voltammetry; EGFET

1. INTRODUCTION

Diseases such as diabetes mellitus are a worldwide concern. Diabetes is a disease related to glucose metabolism that is caused by the lack or poor absorption of insulin, a hormone produced by the pancreas, whose function is to break down glucose molecules to transform them into energy in order to be utilized by all cells. Total or partial absence of the hormone interferes not only in burning sugar but also in its transformation into other substances. It is very important to monitor blood glucose because values outside the range of 80-120 mg/dL (4.4-6.6 mmol/L) can cause problems such as elevated risk of heart disease, kidney failure, or blindness [1,2]. A specific biosensor is needed to

monitor blood glucose levels. At a basic level, a biosensor is a sensor device which converts a response in an electrical signal from biological material. It is a device that has a transducer and a biological component such as an enzyme and other biocomponents.. The biocomponent react with the analyte and this response is transformed into an electrical signal . There remain several disadvantages in glucose determination based on enzyme such as difficult enzyme immobilization or activation, controlled operating conditions such as temperature control, pH optimum, and expensive [3,4]. Due to the high need for highly selective, sensitive and cost effective sensors, efforts have been focused toward production of a new material to be used as an electric signal sensor that presents an improvement in these characteristics. Recently, a lot of thin films have been widely studied as sensing materials in pH sensors, including carbon nanotubes [5], SnO_2 [6], ZnO [7], V_2O_5 xerogels [8], V_2O_5/HDA[9], V_2O_5/WO_3[10,11], V_2O_5/TiO_2[12] and WO_3 [13]. It is understood that these materials are highly attractive in the bioanalytical area for electrode design if they exhibit a pH sensitivityclose to the Nernstian behavior (59.2 mV/pH) [14]. As alternative materials for electric signal sensing, tungsten oxide (WO_3) and vanadium pentoxide (V_2O_5) in xerogel form (comment 2) obtained by sol-gel synthesis are presented. Specifically, WO_3 in xerogel form (comment 2) exhibits hopping conduction between W^{6+} and W^{5+} or W^{5+} and W^{4+} that result in an increase conductivity and carrier mobility [15]. The conduction of WO_3 in xerogel form (comment 2) obtained by the sol-gel synthesis is anisotropic and is proposed to be due mainly to protons, which move through hydrogen bonds across the W–O–W layers [11]. Research on WO_3 in xerogel form (comment 2) has generated significant interest due to its use for detection of gaseous adsorbates [16]. Furthermore, it is amenable to microfabrication techniques [17]. An alternative oxide with potential to be used as an electric signal sensor is V_2O_5 in thin film form obtained by the sol-gel route. The electrical and optical properties of V_2O_5 in xerogel form (comment 2), [18,19] and its lamellar structure make it appropriate for many applications such as catalysis [20], gas sensing [21], as a cathode for Li-ions batteries [22], photosensing in solar cells [23], electrochromic devices [24], as well as electronic and optical switches [25]. Also recently reported in the literature was the use of V_2O_5 and WO_3 xerogels as components in pH-EGFET sensing [8-13]. An extended gate field effect transistor (EGFET) is similar to an ion-selective field effect transistor (ISFET), but the EGFET has an extended gate electrode whose surface potential is controlled due to the presence of a sensitive layer structure [26]. The aim of this work was to prepare an electric signal sensor using vanadium pentoxide xerogel and tungsten oxide, both obtained by the sol-gel route, and to verify whether they are suitable for development of an EGFET glucose biosensor.

2. EXPERIMENTS

The V_2O_5 xerogel was prepared from a solution of 0.1 mol/L of sodium metavanadate ($NaVO_3$, 99%, Fluka). This solution was transferresto the ionic exchange column (ion-exchange resin Dowex-50X8), as described in the literature [27,28]. Decavanadic acid was obtained by percolating a 0.10 mol/L aqueous $NaVO_3$ solution through a cationic ion-exchange resin. This solution (HVO_3) was aged at room temperature (24 °C) for 2 weeks and the solution was polymerized leading to a viscous

red V_2O_5 gel. To prepare the work electrode, the V_2O_5 gel was dropped onto an indium tin oxide (ITO/PET) substrate and dried at room temperature, leading to the formation of a xerogel thin film.

The WO_3 in xerogel form (comment 2) was prepared from sodium tungstate ($NaWO_3$, VETEC) by the ion exchange column (ion-exchange resin Dowex-50X8) as described in the literature [11]. Acid solution was obtained by percolating a 0.1 mol/L aqueous $NaWO_3$ solution. The solution obtained from column was aged for 2 weeks and standing at room temperature (24 °C) . Then, the solution was polymerized, leading to a viscous yellow WO_3 gel. The WO_3 gel was dropped onto an ITO/PET substrate and dried at room temperature, leading to the formation of a xerogel thin film.

Immobilization of GOx was carried out using a 1.5 mg/mL solution of GOx enzyme in a Phosphate Buffer Solution - PBS medium (10 KU by Sigma-Aldrich) mixed with a 5% glutaraldehyde solution over the V_2O_5 and WO_3 xerogels present in the work electrode. The electrode was then dried at 10 °C.

X-ray diffraction (XRD) data were recorded on a SIEMENS D5005 diffractometer using a graphite monochromator and CuK_α emission line (1.541 Å, 40 kV, 40 mA). Data were collected at room temperature over the range $2° \leq 2\theta \leq 50°$, with a step of 0.020°. The images were obtained from Scanning Electron Microscopy (SEM) using a ZEISS microscope EVO 50 model operating at 20 kV. A thin gold coating (≈ 20 Å) was applied to the sample using a Sputter Coater – Balzers SCD 050. The length of the platelet particles was determined using the ImageTools® software.

The electrical response of the sensor was measured using varying pH solutions. The curves were obtained using an Agilent 34970A parameter analyzer. The electrode with the film coating was dipped into a PBS, containing 1 mmol/L of glucose (Sigma) (comments 5 and 6) at room temperature for 5 minutes prior to the electrical measurement. Voltammograms were measured using an AUTOLAB (MetrohmPensalab) model μAutolabIII (Nova 1.10) potentiostat/galvanostat. The conventional electrode arrangement was used, which consisted of PET/ITO as the working electrode, a platinum wire auxiliary electrode, and a saturated calomel electrode (SCE) as the reference. The WO_3 and V_2O_5 thin films were deposited on the electrode surface by evaporating approximately 5 mL of the suspension at room temperature (24 °C). PBS with 1 mmol/L of glucose and different pH values were used as the supporting electrolyte (comments 5 and 6).

3. RESULTS AND DISCUSSION

The oxides prepared by the sol-gel route were characterized by X-ray diffraction (XRD), which confirmed the formation of V_2O_5 and WO_3, both with a lamellar structure. Figure 1 shows the XRD pattern for V_2O_5 in xerogel form (comment 2).

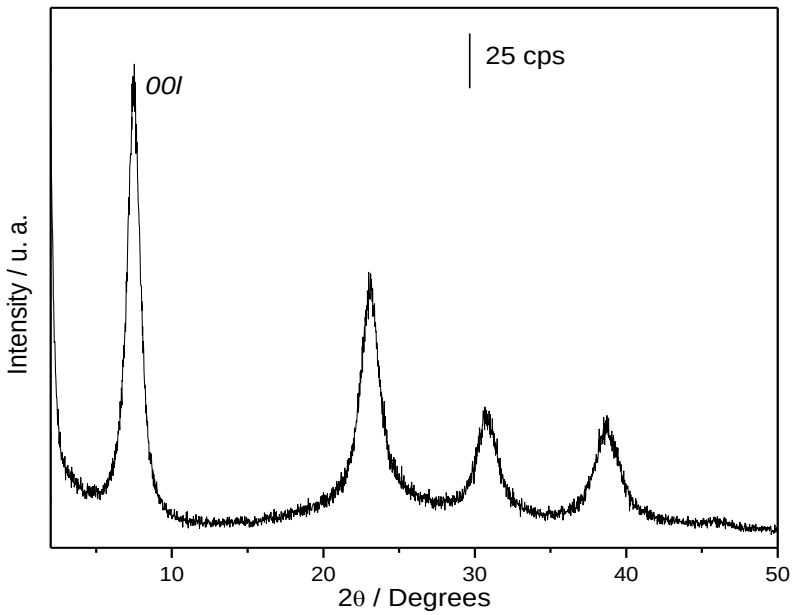

Figure 1. Diffractogram of V_2O_5 in xerogel form (comment 2).

The diffractogram (Figure 1) shows the strongest diffraction peak (00l), which arises from the one dimensional stacking of the V_2O_5 in xerogel form (comment 2) ribbons that are perpendicular to the substrate, [29] as observed in Figure 2. The V-O interlayers are formed by tangled fibers and connected by water molecules present in the structure [30]. Furthermore, the typical equidistant diffraction peaks observed in the XRD pattern is observed and it can be indicate a formation of layered structure, indicating that the lamellar structure of the V_2O_5 in xerogel form is kept after the drying process. In addition, the interlayer spacing of d = 1.17 nm, suggests a ratio of n = 1.8 of water molecules are intercalated between these ribbons resulting in $V_2O_5.1.8H_2O$, as also observed in the literature [31].

Morphological studies of V_2O_5 in xerogel form were published recently [8]. Based on the literature [32], V_2O_5 in xerogel form (comment 2) consists of entangled fibers that can be described as long flat ribbons exhibiting a bidimensional structure. Additionally, V_2O_5 in xerogel form (comment 2) consists of polymeric chains obtained by the autocatalytic process during olation and oxolation. Concerning the relative orientation of the stacked layers there is no preference. As observed in Figure 3, the distance between the layers is well defined and depends on the amount of intercalated water molecules. According to the literature [34], during the structural evolution that occurs with the gelation of vanadic acid, the formation of small whisker-like particles from the initial solution precedes the appearance of the fibrous colloidal species, which is consistent with a nucleation and growth process.

From the SEM image of V_2O_5 in xerogel form (comment 2) (Figure 2), it is possible to observe the presence of interconnected clusters, fibrils, and ribbons, forming a network of chains. These clusters may be associated with nucleation centers. The growth is promoted by a grain in a first stage and, in a second stage, the formation and growth of ribbons and fibrils takes place, thereby promoting the organization of the polymeric chains in the oxide. The ribbons, formed by the condensation process

of vanadic acid, likely consist of corner-sharing VO_5 pyramids, and the growth takes place in the addition of dioxovanadium cations. The matrix grows radially during the formation process of $V_2O_5.nH_2O$, forming a spherulite structure of polymeric chains. This type of structure consists of a crystal array and amorphous regions linked together, generated from a nucleation center [33].

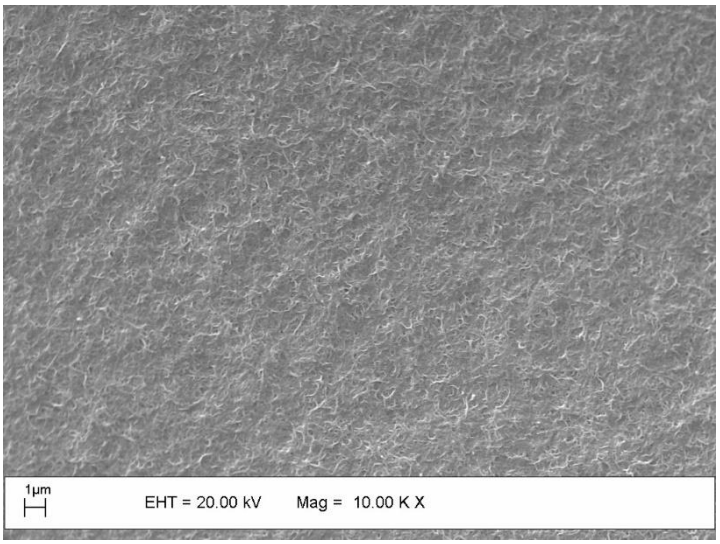

Figure 2. SEM image of V_2O_5 in xerogel form (comment 2)

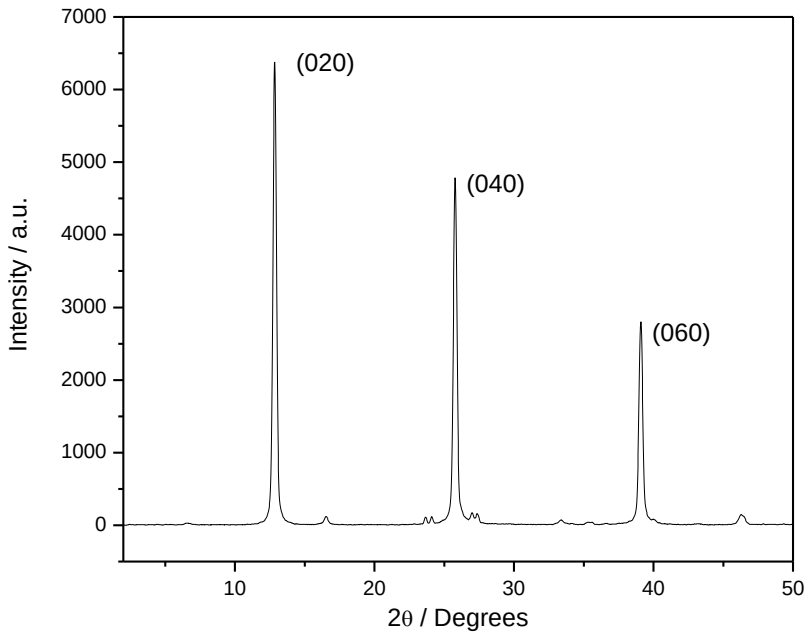

Figure 3. Diffractogram of WO_3 in xerogel form (comment 2).

Figure 3 shows the X-ray diffraction pattern for WO_3 in xerogel form (comment 2). The diffractogram exhibits a series of harmonic peaks that can be indexed as *0k0*, according to the lamellar structure of WO_3. Therefore, the *0k0* index represents to the stacking of plate-like particles along a

direction perpendicular to the substrate. Additionally, the peaks indicate that the lamellar structure of WO_3 is not changedafter the drying process, as observed in Figure 4. Based on Bragg´s law, the interlayer spacing, *d*, between the platelets (*d* = 0.69 nm) suggests that water molecules (n = 2) are intercalated between these platelets resulting in $WO_3.2H_2O$, as observed in the literature [34]. The diffraction peaks exhibit high intensity and narrow width, suggesting that this material has high crystallinity.

Figure 4 shows the SEM image of WO_3 in xerogel form (comment 2). As observed, a process corresponding to the separation of stacked inorganic sheets occurred during WO_3 formation. The crystallites of the material consist of irregularly stacked rounded platelets with length of approximately 10–20 nm and thickness less than 1.0 nm, as shown in Figure 4.

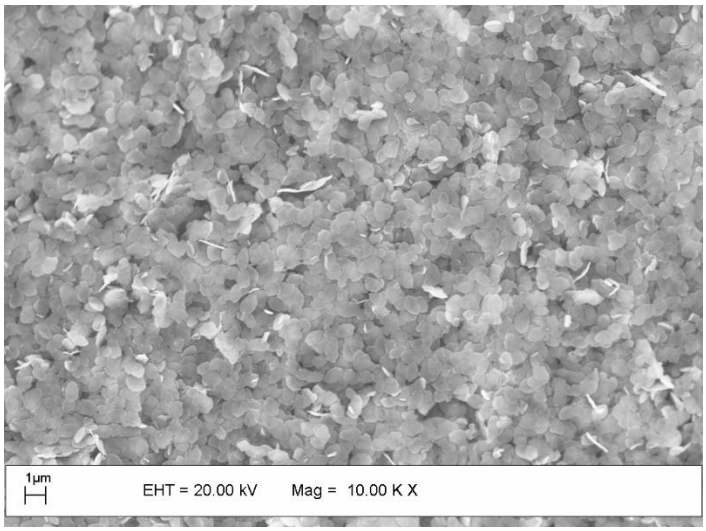

Figure 4. SEM image of WO_3 in xerogel form (comment 2)

Figure 5 shows the response of an EGFET system using V_2O_5 in xerogel form (comment 2) as the extended gate. GOx was immobilized onto the surface of the oxide and the sensor was tested in the presence and absence of glucose.

It is observed that all current measurements corresponding to the medium lacking glucose are higher than 5.30 mA. Furthermore, the current measured for each sensor decreased with ascending pH with the exception of pH = 7.58. Note that the measured current is higher in the presence of glucose for each pH value tested, which indicates the operation of the oxidoreductase enzyme in the catalysis process This result may be related to presence of V_2O_5 as a sensing component that promotes faster electron transfer between the enzyme and electrode, leading to an increase in the measured current. This increase in current can also be attributed to the redox reactions at actives site of the immobilized GOx, which results in a synergetic effect between V_2O_5 and the enzyme [35].

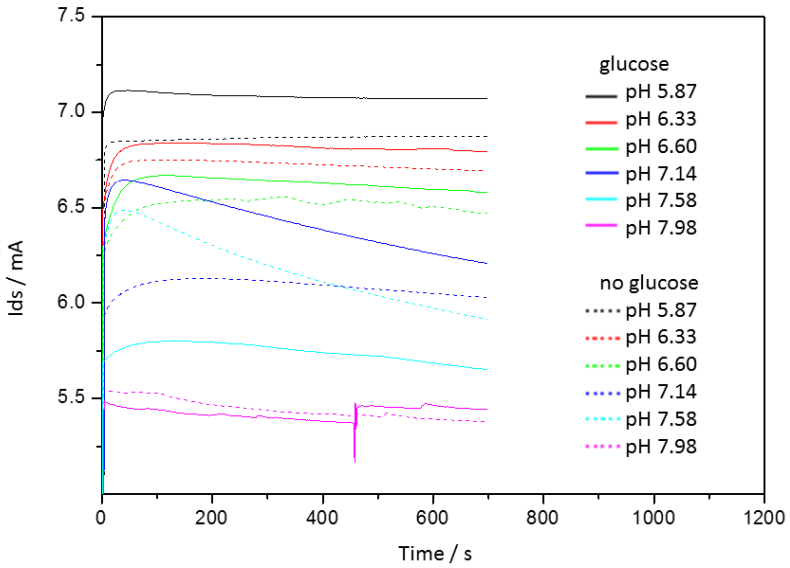

Figure 5. Drain-source current as a function of time of V_2O_5/GOx for varying pH values in 1 mmol/L glucose.

The dashed lines in Figure 6 correspond to the sensor in a PBS solution while the solid lines correspond to the sensor in a PBS solution with 1 mmol/L glucose. The adopted enzyme pH working range was 5.5 to 7.8 with the optimal pH between 4 and 7, according to the manufacturer (Sigma-Aldrich). Figure 6 shows that the working range for the immobilized enzyme is restricted to 5.9 to 6.1, where it exhibited a higher current value.

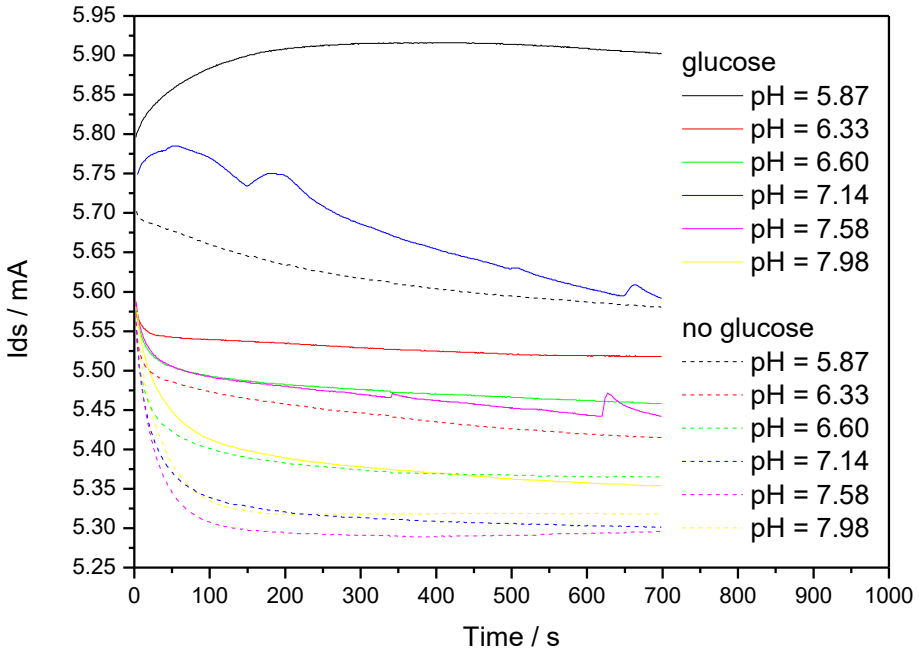

Figure 6. Drain-source current as a function of time for WO_3/GOx at varying pH values in 1 mmol/L glucose

When the pH is lower than 5.9, the enzyme loses its activity (close to 300 ms). For pH greater than 6.1 the enzyme no longer works, not exhibiting activity at pH close to 7.8, likely due to irreversible denaturation, as will occur in strong acidic or alkaline medium conditions. Several parameters may promote the total enzyme catalytic activity. The pH, the substrate and, consequently, its combination are important parameters that influence the general reaction mechanism [36, 37]. Based on these observations, we conclude that the working range for immobilized GOx is restricted to pH 5.9-6.2.. Therefore, pH = 6.1 was used for subsequent electrochemical studies.

In Figure 7, glucose is present in the electrolyte. Its presence results in an enzyme-catalyzed reaction that decreases the concentration of the oxidized form of GOx on the electrode surface.

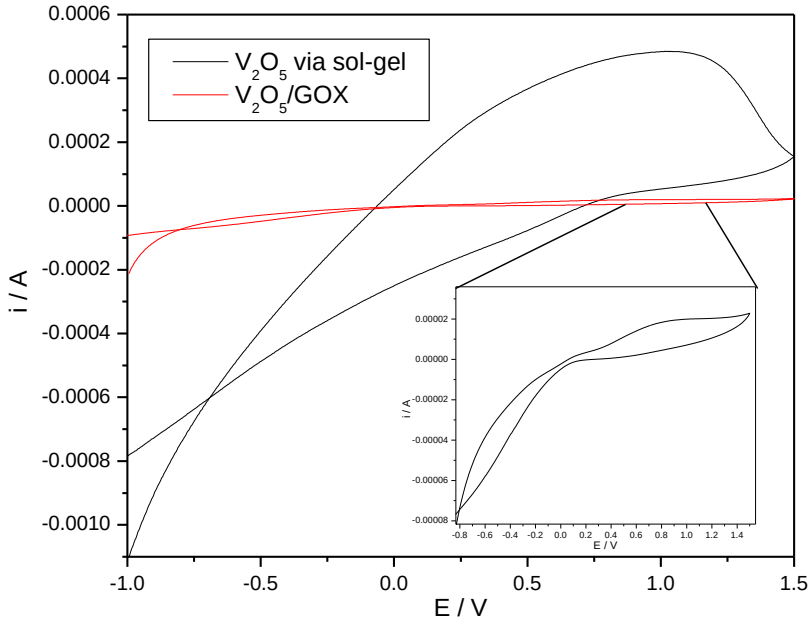

Figure 7. Cyclic voltammograms of V_2O_5 in xerogel form (comment 2) and V_2O_5/GOx in 1 mmol/L glucose in PBS solution with pH = 6.1

Thus, the addition of glucose limited the electrocatalytic reaction and led to a decrease in reduction current. Upon addition of glucose, the electrocatalytic reaction is limited to the enzyme-catalyzed reaction between the oxidized form of GOx and glucose [38,39]. As shown in Figure 7, a single, stable and well defined redox peak for the direct electron transfer of GOx can be observed in the cyclic sweep of the V_2O_5 in xerogel form and V_2O_5/GOx working electrodes in 0.1 mmol/L pH 6.1 PBS. For V_2O_5/GOx working electrode, the anodic peak potential was 1.04 V and cathodic peak was 0.48 V, both at 20 mV/s. When GOx was immobilized on the surface of V_2O_5, the cyclic voltammogram showed an anodic potential shift toward negative values, at 0.83 V, (Figure 7, red line) indicating that the immobilization of GOx as well as the direct electron transfer of GOx were favorable. The decrease in reduction current after GOx immobilization onto V_2O_5 may be due to the smaller number of active sites on electrode surface. Comparing V_2O_5 and GOx, the oxide presents a larger number of active sites per cm^2 than GOx. This fact may lead to the reduction in electron

exchange between the GOx and V_2O_5 and, consequently, to the decrease in current after immobilization of GOx on V_2O_5 [40].

Figure 8 shows the cyclic voltammograms before and after immobilization of GOx on WO_3. In the cyclic voltammogram of WO_3 in PBS at pH = 6.1, it was possible to observe an anodic peak at -0.42 V at 20 mV/s. After GOx immobilization onto WO_3, a single anodic peak at -0.53 V was observed in presence of 1.0 mmol/L glucose, indicating direct electron transfer between GOx and the electrode. Comparing WO_3 to V_2O_5 it is possible to conclude that the decrease in current is also due to the decrease in active sites present in the GOx sample when compared to WO_3 alone.

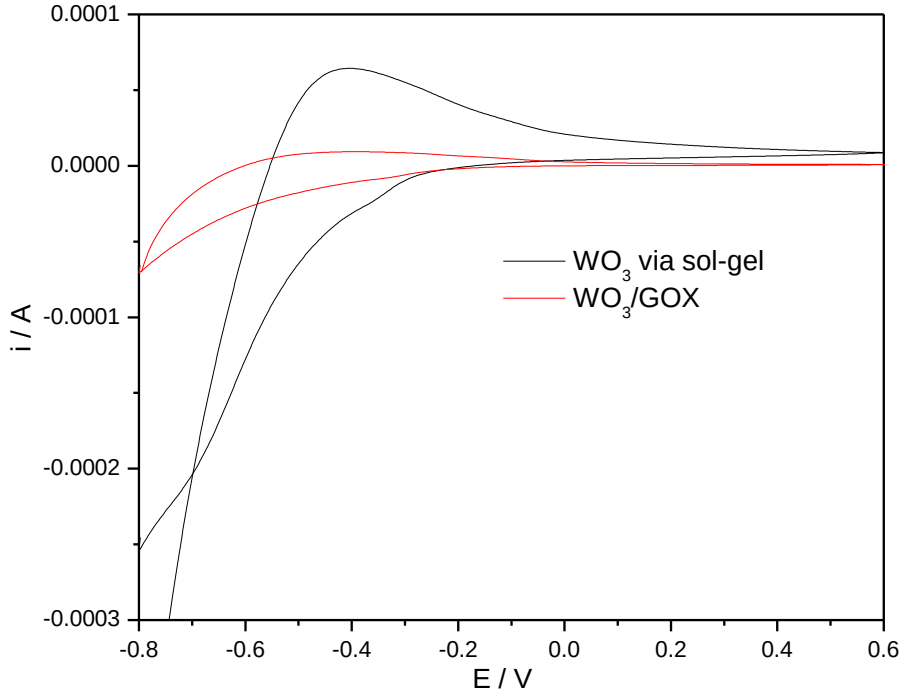

Figure 8. Cyclic voltammograms of WO_3 in xerogel form (comment 2) and WO_3/GOx in 1 mmol/L glucose in PBS solution with pH = 6.1

GOx presents a cavity that constitutes the substrate binding site. This cavity, which is located in the center of the enzyme, interacts with each of the five hydroxyl groups of glucose. Thus, the glucose is tightly bound at the active site of each 80 kDa subunit of GOx [41]. As is well known, bridging V-O-V and W-O-W groups in two-dimensional arrays favored at high vanadium and tungsten coverages have been proposed as active sites [42]. Based on these facts, the electrocatalytic reaction after addition of GOx onto the oxides will exhibit a decrease in current.

4. CONCLUSION

It was demonstrated that vanadium pentoxide and tungsten oxide, prepared via sol-gel route, exhibit a lamellar structure, as evidenced by X-ray diffraction data. SEM showed that crystallites of WO_3 in xerogel form (comment 2) consist of an irregular rounded platelets stacking with length of approximately 10–20 nm and thickness less than 1.0 nm. V_2O_5 in xerogel form (comment 2) was

observed to be comprised of ribbons formed by the condensation process of vanadic acid. These structures made the immobilization of GOx favorable for both oxides, as confirmed by the EGFET and electrochemical studies of glucose detection. Thus, these materials have potential for application as biosensors for detection of glucose. Further, studies using different parameters such as variation of glucose concentration, different pH and other electrochemical techniques are required in the future.

ACKNOWLEDGEMENT
This work was supported by FAPEMIG, FAPESP, INEO, CNPq and CAPES Brazilian agencies.

References

1. M. M. W. Muscatello, L. E. Stunja, S. A. Asher, *Anal. Chem.* 81, (2009) 4978–4986.
2. D. Odaci, B. N. Gacal, B. Gacal, S. Timur, Y. Yagci, *Biomacromol.*, 10 (2009) 2928.
3. E. Reitz, W. Jia, M. Gentile, Y. Wang, Y. Lei, *Electroanal.*, 20 (2008) 2482.
4. N. Sachedina, J. C. Pickup, *Diabet. Med.*, 20 (2003) 1012.
5. G. R. Silva, E. Y. Matsubara, P. Corio, J. M. Rosolen, M. Mulato, *MRS Proc*., 1018 (2007).
6. P. D. Batista, M. Mulato, C. F. O. Graeff, F. J. R. Fernandez, F. Dias, C. Marques, *Brazilian J. Phys.*, 36 (2006) 478.
7. P. D. Batista, M. Mulato, *Appl. Phys. Lett.*, 87 (2005) 143508.
8. E. M. Guerra, G. R. Silva, M. Mulato, *Solid State Sci.*, 11 (2009) 456.
9. E. M. Guerra, M. Mulato, *J. Sol-Gel Sci. Technol.*, 52 (2009) 315.
10. E. J. Guidelli, E. M. Guerra, M. Mulato, *ECS J. Solid State Sci. Technol.*, 1 (2012) N39.
11. E. J. Guidelli, E. M. Guerra, M. Mulato, *Mater. Chem. Phys.*, 125 (2011) 833.
12. E. J. Guidelli, E. M. Guerra, M. Mulato, *J. Electrochem. Soc*., 159 (2012) J217.
13. R. C. De Campos, D. T. Cestarolli, M. Mulato, E. M. Guerra, *Mater. Res*., 18 (2015) 15.
14. M. J. Schöning, A. Simonis, C. Ruge, H. Ecken, M. Müller-Veggian, H. Lüth, *Sensors*, 2 (2002) 11.
15. X. Li, Q. Zhang, W. Miao, L. Huang, Z. Zhang, Z. Hua, *J. Vac. Sci. Technol. A Vacuum, Surfaces, Film*, 24 (2006) 1866.
16. D.-S. Lee, K.-H. Nam, D.-D. Lee, *Thin Solid Films*, 375 (2000) 142.
17. G. Wang, Y. Ji, X. Huang, X. Yang, P.-I. Gouma, M. Dudley, *J. Phys. Chem. B.*, 110 (2006) 23777.
18. A. A. Bahgat, F. A. Ibrahim, M. M. El-Desoky, *Thin Solid Films*, 489 (2005) 68.
19. E. M. Guerra, C. A. Brunello, C. F. O. Graeff, H. P. Oliveira, *J. Solid State Chem.*, 168 (2002) 134.
20. M. E. Manríquez, G. Morales-Mendoza, J. Alamilla, U. Trejo, R. Gómez, E. Ortiz-Islas, *Reac. Kinet. Mech. Cat.*, 122 (2017) 1281.
21. K. Schneider, M. Lubecka, A. Czapla, *Sens. Actuat. B*, 236 (2016) 970.
22. M. Haris, S. Atiq, S. M. Abbas, A. Mahmood, S. M. Ramay, S. Naseem, *J. Alloys and Comp.*, 732 (2018) 518.
23. G. E. Silva, K. V. S. Oliveira, R. F. Bianchi, D. T. Cestarolli, E. M. Guerra, *Photovolt. Spec. Conf.*, (2015)
24. Y. X. Wei, Y. B. Ma, M. Chen, W. M. Liu, L. Li, Y. Yan, J. Electroanalyt. Chem., 807 (2017) 45.
25. S. Saitzek, F. Guinneton, G. Guirleo, L. Sauques, K. Aguir, J.-R. Gavarri, *Thin Solid Films*, 516 (2008) 891.
26. J. van der Spiegel, I. Lauks, P. Chan, D. Babic, *Sensors and Actuators*, 4 (1983) 291.
27. N. Gharbi, C. Sanchez, J. Livage, J. Lemerle, L. Nejem, J. Lefebvre, *Inorg. Chem.*, 21 (1982) 2758.
28. J. Livage, *Chem. Mater*., 3 (1991) 578.

29. V. Petkov, P. N. Trikalitis, E. S. Bozin, S. J. L. Billinge, T. Vogt, M. G. Kanatzidis, *J. Am. Chem. Soc*., 124 (2002) 10157.
30. G. S. Zakharova, V. L. Volkov, *Russ. Chem. Rev*., 72 (2003) 311.
31. P. Aldebert, N. Baffier, N. Gharbi, J. Livage, *Mater. Res. Bull.*, 16 (1981) 669.
32. R. Baddour, J. P. Pereira-Ramos, R. Messina, J. Perichon, *J. Electroanal. Chem. Interfacial Electrochem.*, 314 (1991) 81.
33. J. K. Bailey, G. A. Pozarnsky, M. L. Mecartney, *J. Mater. Res.*, 7 (1992) 2530.
34. A. Chemseddine, F. Babonneau, J. Livage, *J. Non. Cryst. Solids*., 91 (1987) 271.
35. N. Sanaeifar, M. Rabiee, M. Abdolrahim, M. Tahriri, D. Vashaee, L. Tayebi, *Anal. Biochem.*, 519 (2017) 19.
36. M. K. Weibel, H. J. Brights, *J. Biol. Chem.*, 246 (1971) 2734.
37. H. J. Brights, M. Appleby, *J. Biol. Chem.*, 244 (1969) 3625.
38. P. De Taxis, D. Poet, S. Miyamoto, T. Murakami, J. Kimura, I. Karube, *Anal. Chim. Acta*, 235 (1990) 255.
39. R. Garjonyte, A. Malinauskas, *Biosens. Bioelectron.*, 15 (2000) 445.
40. S. Liu, H. Ju, *Biosens. Bioelectron.*, 19 (2003) 177.
41. S. Ferri, K. Kojima, K. Sode, *J. Diabetes Sci. Technol.*, 5 (2011) 1068.
42. J. Eon, *J. Catal.*, 145 (1994) 318